Scientific Research Publishing

Open Journal of Applied Sciences, 2026, 16(1), 247-261
https://www.scirp.org/journal/ojapps
ISSN Online: 2165-3925
ISSN Print: 2165-3917

Fatigue Life Prediction of Vehicle Rubber Elastic Support Components Based on Physics-Informed Neural Networks

Shen Liu*, Fei Meng#

Science of Systems, University of Shanghai for Science and Technology, Shanghai, China
Email: #feimeng@usst.edu.cn

How to cite this paper: Liu, S. and Meng, F. (2026) Fatigue Life Prediction of Vehicle Rubber Elastic Support Components Based on Physics-Informed Neural Networks. *Open Journal of Applied Sciences*, **16**, 247-261.
https://doi.org/10.4236/ojapps.2026.161015

Received: December 22, 2025
Accepted: January 16, 2026
Published: January 19, 2026

Abstract

Rubber is widely used in automotive vibration isolation systems due to its excellent mechanical properties and durability. However, elastomeric support components tend to experience performance degradation under high-temperature and cyclic loading conditions. Consequently, predicting the fatigue life of these components has been a critical issue in structural reliability research. Due to the strong nonlinearity and significant energy dissipation characteristics of rubber, traditional empirical models are often limited by small sample sizes and lack physical interpretability, making it difficult to accurately describe the damage evolution process under complex operating conditions. To enhance the reliability of fatigue predictions, this study proposes a modeling approach based on Physics-Informed Neural Networks (PINN). By integrating physical modeling with data-driven techniques and embedding damage evolution equations into the learning framework, the model not only adheres to physical laws but also fits the measured stiffness degradation curves, even with limited experimental data. The results show that this method effectively reconstructs the material's fatigue damage process and reliably predicts its fatigue life. The proposed PINN framework offers an efficient and physically consistent approach for evaluating the fatigue life of rubber-based support components.

Keywords

Data-Driven Model, Fatigue Life, PINN Model, Rubber Isolators, Stiffness

1. Introduction

Rubber is widely used in automotive vibration isolation systems due to its excel-

*First author.
#Corresponding author.

lent performance as a non-metallic material [1]-[3]. Elastic support components are key to vibration isolation. However, under long-term cyclic loading, rubber materials experience stiffness degradation and fatigue damage, leading to component failure. This threatens vehicle reliability and NVH performance [4]. Thus, predicting the high-temperature fatigue life of rubber elastic support components is important for structural reliability. Rubber materials have significant nonlinearity, viscoelasticity, and temperature sensitivity. Their fatigue behavior is influenced by factors such as load, temperature, and internal damage. This limits the use of traditional S-N curves and continuous damage models in real engineering scenarios [5]. Additionally, rubber fatigue testing is costly and time-consuming. It is hard to gather large quantities of high-quality fatigue data, limiting the application of empirical or data-driven models.

With the rise of artificial intelligence and machine learning, neural networks, particularly Artificial Neural Networks (ANN), have become key tools for predicting rubber fatigue life [6]. ANN can train on large datasets to build complex models. These models address nonlinear and high-dimensional problems that traditional models cannot, improving accuracy [7]. Liu *et al.* [8] [9] used peak strain, temperature, and material hardness as inputs to predict fatigue life. They used an ELM model and cosine-optimized BPNN. Similarly, Liu *et al.* [10] created an ANN model to predict the fatigue life of natural rubber (NR) under different conditions. Traditional rubber fatigue life predictions rely on empirical models [11]-[13] or continuous damage mechanics [14]. These methods need large datasets, which are hard to obtain due to cost and time constraints. Models with limited data often face poor physical interpretability, overfitting, and extrapolation errors [15].

Recently, Physics-Informed Neural Networks (PINN) have been applied to material fatigue life predictions [16]. PINN combines physical models with data-driven techniques. By embedding damage evolution equations in the network, PINN follows physical laws while fitting experimental data with limited samples [17]. This approach works well when large datasets are unavailable. For example, Wang *et al.* [18] integrated defect characteristics of additive manufacturing materials into an ANN model to predict fatigue life. Halamka *et al.* [19] and Wang *et al.* [20] used PINN to improve the accuracy of metal fatigue life predictions by combining physical data with ANN. Chen *et al.* [21] applied multi-fidelity PINN for metal fatigue life predictions, improving extrapolation accuracy with just 18 - 31 samples. Dong *et al.* [22] developed a fracture mechanics-based PINN to predict material life with defects. Many studies have combined physical models with machine learning for fatigue life prediction in metals and polymers [23] [24]. The fatigue life theory for natural rubber (NR) components is still under development.

Based on this research, we propose a PINN-based framework to predict the fatigue life of rubber elastic support components. The method uses a strain energy density-driven damage evolution equation as the physical prior and experimental stiffness degradation data as constraints. This ensures the model follows physical

laws and fits measured data with small samples. Our PINN, with physical constraints, shows lower RMSE and higher R^2 than purely data-driven models. This approach offers a data-efficient, interpretable solution for the reliability design of rubber-based components.

This paper is organized as follows: Section 2 presents the principles and architecture of BPNN and PINN models. Section 3 introduces the experimental setup, data collection methods, and processing procedures. Section 4 compares the prediction performance of the BPNN and PINN models. Finally, Section 5 summarizes the main findings and conclusions.

2. Methodology

2.1. Data-Driven Mode

Backpropagation Neural Network (BPNN) is a data-driven model that utilizes gradient descent algorithms to enhance its performance. Through the backpropagation process, BPNN adjusts the connection weights between multiple layers of neurons, effectively capturing and predicting nonlinear relationships [25]. This capability has led to its widespread application in fatigue life prediction.

The BPNN architecture processes input features, including the number of cycles N, stress, and strain to generate the predicted stiffness. The input features are not normalized in order to preserve their physical meaning; however, training efficiency is ensured by carefully tuning the learning rate. The input and output for the hidden layer are computed as follows:

$$\text{Input:}\quad \kappa_j = \sum_{i=1}^{3} \omega_i x_i + b_i \tag{1}$$

where $j = 1, 2, \cdots, n$, ω_i represents the weight coefficient connecting the i^{th} input neuron to the j^{th} neuron in the hidden layer, and b_i is the bias parameter associated with the j^{th} neuron.

$$\text{Output:}\quad d_j = F\left(\kappa_j\right) \tag{2}$$

where $F(\cdot)$ is the activation function. The activation function adopted in this study is the rectified linear unit (ReLU), defined as:

$$F(x) = \max(0, x) \tag{3}$$

with its derivative:

$$F'(x) = \begin{cases} 1, & \text{if } x > 0 \\ 0, & \text{if } x \le 0 \end{cases}. \tag{4}$$

The input and output for the output layer are given by:

$$\text{Input:}\quad \xi = \sum_{j=1}^{n} v_j d_j + \varphi, \tag{5}$$

$$\text{Output:}\quad \hat{y} = \xi, \tag{6}$$

where v_j denotes the weight coefficient connecting the hidden layer to the output layer, and φ is the bias parameter controlling the activation of the output

neuron.

The BPNN training process involves error backpropagation, where the error is propagated from the output layer to the hidden layer. The errors for the output and hidden layers are calculated as:

$$\text{Output layer:}\quad \delta_k = t_k - \hat{y}_k, \tag{7}$$

$$\text{Hidden layer:}\quad \delta_j = \left(\sum_k \delta_k \upsilon_{kj}\right) \cdot \begin{cases} 1, & k_j > 0 \\ 0, & k_j \le 0 \end{cases} \tag{8}$$

In this study, the BPNN model utilizes the adaptive moment estimation (Adam) optimization algorithm for the backpropagation process. Adam combines the advantages of momentum-based gradient descent and root mean square propagation (RMSProp), ensuring efficient convergence. A grid search method based on 10-fold cross-validation was employed to select the model's hyperparameters. The optimal hyperparameters and architecture for the BPNN model were determined. The optimal number of hidden layers was set to 4, with 30 neurons in each layer. The epoch and learning rate were set to 2000 and 0.005, respectively.

2.2. Physics-Informed Neural Network (PINN)

In the fatigue life prediction of rubber materials, traditional empirical models and data-driven models often exhibit certain limitations. To address this issue, this study proposes a fatigue life prediction method based on Physics-Informed Neural Networks (PINN). PINN integrates physical modeling with data-driven techniques, enabling the model to learn a damage evolution process that adheres to physical laws by incorporating physical constraints. This approach allows for accurate fatigue life and stiffness degradation predictions even with limited experimental data [26].

The structure of the Physics-Informed Neural Network (PINN) based on strain energy density is shown in **Figure 1**. The stiffness data, load, and cycle number obtained from the experimental setup are used as inputs to the PINN model, with the predicted stiffness degradation serving as the output. The hyperparameters are determined through a grid search method based on 10-fold cross-validation. The optimal architecture was found to consist of four hidden layers, each containing 30 neurons. The number of training epochs and learning rate were set to 2000 and 0.005, respectively. The optimization process employs the Adam optimizer algorithm. The damage evolution equation and stiffness degradation model are embedded in the neural network training process, ensuring that the network's output not only fits the experimental data but also adheres to known physical laws. Specifically, PINN uses the damage evolution equation (based on energy dissipation) as a physical constraint and fits the damage variable and stiffness through the neural network to establish the damage evolution equation, as follows:

$$\frac{\mathrm{d}D}{\mathrm{d}N} = \alpha W^m \left(1 - D\right)^p \tag{9}$$

where, D represents the damage variable, N is the number of cycles, W is

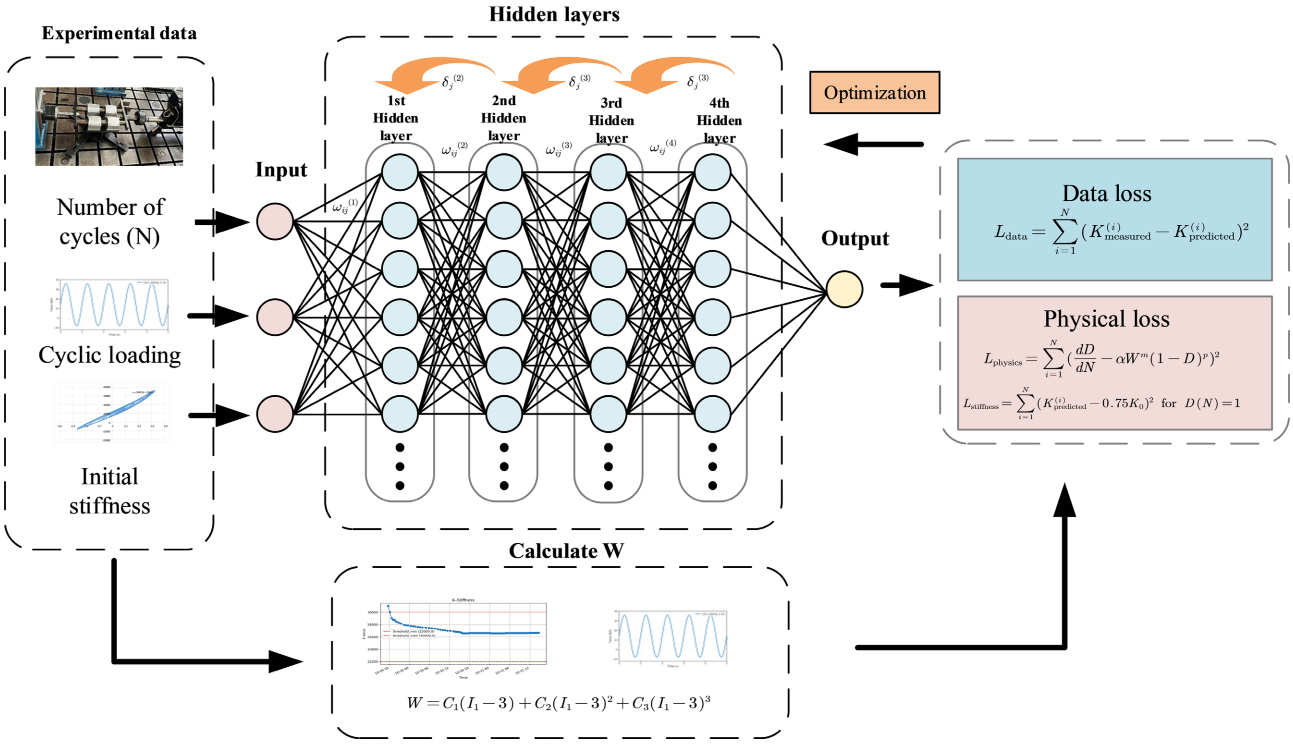

Figure 1. The architecture of the Physics-Informed Neural Network (PINN) based on strain energy density.

the strain energy density, the damage parameters α and β are treated as learnable parameters that are optimized simultaneously with the neural network weights during the training of the Physics-Informed Neural Network (PINN). This approach enables the model to adaptively adjust the damage evolution equation based on experimental data, rather than relying on predefined values obtained from prior curve fitting. Consequently, it enhances the flexibility of the physical constraints and improves the predictive accuracy of the model. Strain energy density (W) is a key physical quantity that describes the energy dissipation of materials. It is closely related to both the stiffness degradation and fatigue damage of the material. In this study, the strain energy density is calculated using the Yeoh model, which is suitable for modeling the large deformation behavior of materials such as rubber. The strain energy density formula of the Yeoh model is as follows:

$$W = C_1(I_1 - 3) + C_2(I_1 - 3)^2 + C_3(I_1 - 3)^3 \tag{10}$$

where, I_1 represents the first invariant of the right Cauchy-Green deformation tensor, and C_1, C_2, and C_3 are material constants obtained through experimental data fitting. The Yeoh model accurately describes the nonlinear large deformation behavior of rubber materials and calculates the strain energy density. For the material used in the experiments, the constants are as follows: $C_1 = 2.96$ MPa, $C_2 = 4.37$ MPa, and $C_3 = 3.19$ MPa [27].

By calculating the stiffness variation curve and load data, the strain energy density W is computed, providing the necessary input for the damage evolution

equation. During the fatigue process, the stiffness of rubber materials gradually degrades with the increase in the damage variable D. A commonly used relationship is:

$$K(N) = K_0\left(1 - D(N)\right) \tag{11}$$

where, $K(N)$ represents the material stiffness after the N-th cycle, K_0 is the initial stiffness, and $D(N)$ is the damage variable that describes the degree of fatigue damage in the material.

There is no unified standard for fatigue failure criteria of rubber materials. Previous studies have used static stiffness degradation as a key indicator of fatigue damage [28]. Literature [29] reports that rubber materials exhibit significant static stiffness reduction after fatigue loading. According to the TB/T 2843 standard, the tolerance limits for static property changes of rubber elastic components after fatigue are ±20% for strict tolerance and ±30% for normal tolerance. Based on the service requirements of actual vehicle suspension structures and engineering experience, this study adopts a 25% reduction in static stiffness as the fatigue failure criterion, which is expressed by the following formula:

$$\Delta K = \frac{K_0 - K_f}{K_0} \times 100\% \tag{12}$$

where, ΔK represents the static stiffness degradation rate, K_0 is the initial static stiffness, and K_f is the static stiffness after fatigue.

To ensure that the model training adheres to physical laws, it is necessary to specify the initial and boundary conditions. The initial condition is that the damage variable $D_0 = 0$, indicating that the material is undamaged at the initial time. The initial stiffness K_0 is obtained from experimental data. The boundary condition is that when the stiffness degrades to 25%, the damage variable D reaches its maximum value of 1.

The loss function of the PINN model consists of two components: data loss and physical loss. The data loss ensures that the network's predicted stiffness aligns with the experimental data. The data loss is given by the following formula:

$$L_{\text{data}} = \sum_{i=1}^{N}\left(K_{\text{measured}}^{(i)} - K_{\text{predicted}}^{(i)}\right)^2 \tag{13}$$

where K_{measured} is the stiffness experimentally measured, and $K_{\text{predicted}}$ is the stiffness predicted by the model.

The prior physical knowledge of fatigue failure is incorporated into the training process. During training, if the fatigue life prediction contradicts the physical knowledge, the loss function should impose the corresponding physical constraints. The physical loss is given by the following formula:

$$L_{\text{physics}} = \sum_{i=1}^{N}\left(\frac{\mathrm{d}D}{\mathrm{d}N} - \alpha W^m\left(1 - D\right)^p\right)^2 \tag{14}$$

This loss term ensures that the damage variable D follows the damage evolution equation. When the stiffness degrades by 25%, the damage reaches its maxi-

mum value:

$$L_{\text{stiffness}} = \sum_{i=1}^{N} \left(K_{\text{predicted}}^{(i)} - 0.75K_0 \right)^2 \quad \text{for } D(N) = 1 \tag{15}$$

During training, the network computes the damage variable D and stiffness K through forward propagation. The network weights are then updated based on the data loss and physical loss. Through iterative training, the network is able to provide more accurate fatigue life and stiffness predictions by utilizing physical constraints, even with limited data.

To balance the influence of the data loss, physics loss, and boundary condition loss during the optimization process, weighted coefficients are applied to these loss terms. Specifically, the weight for the data loss is set to 1, while the weights for the physics loss and boundary condition loss are determined through grid search optimization as 0.4 and 0.3, respectively. This weighting strategy helps prevent any single loss term from dominating the training process, ensuring that the model fits the experimental data while strictly adhering to physical constraints, thereby improving convergence stability and predictive performance.

The major advantage of PINN lies in its ability to effectively fit the model in data-scarce situations by incorporating physical constraints, thus avoiding overfitting while enhancing the model's generalization capability. Compared to traditional purely data-driven models, PINN better handles small sample problems and ensures physical consistency, thereby improving the accuracy of fatigue life predictions.

3. Experiment Set-Up

This study focuses on a specific type of rubber elastic support component. A uniaxial fatigue test rig for the elastic support specimen was built, as shown in Figure 2. The test rig consists of a hydraulic servo system (MTS-793, MTS Systems Corporation, USA), a force sensor, a heating/air-cooling temperature control system (shown in Figure 3), and the elastic support specimen under test. The

Figure 2. Uniaxial fatigue test rig for elastic support specimen.

Figure 3. Air-heating/air-cooling temperature control system.

hydraulic servo system applies vertical cyclic loads via a hydraulic actuator, allowing precise control of the loading waveform, frequency, and load amplitude. The force sensor continuously monitors the load applied to the specimen and provides feedback for closed-loop control. The temperature control system maintains the specimen surface temperature at 90˚C, simulating the thermal environment near the actual powertrain.

During the experiment, cyclic loading is applied to the specimen based on the load spectrum generated from real vehicle data. Static compression tests are performed at specific cycle points to obtain the evolution of stiffness with respect to the number of loading cycles, enabling the characterization of the fatigue damage process and life prediction.

Data Acquisition and Processing

Table 1. Data collection.

Specimen ID	Loading Amplitude Range (KN)	Stiffness Sampling Interval	Measured fatigue life (no. of cycles)
S1	6 - 36	100,000	9,856,515
S2	−6 - 36	100,000	6,140,050
S3	−6 - 36	50,000	5,621,000
S4	−6 - 36	100,000	5,920,054
S5	−8 - 36	100,000	3,905,455
S6	−8 - 36	100,000	399,525
S7	−8 - 36	50,000	465,250

Table 1 presents the key data for the experimental specimens, including the loading amplitude range, stiffness sampling interval, and measured fatigue life. During the fatigue loading phase, the high-precision force sensor and displace-

ment encoder of the testing machine record the force-displacement response of each loading cycle in real time. This data is used to train the PINN model and calculate the dissipated energy for each cycle.

To reflect the stiffness degradation behavior of the material during the fatigue damage process, the experiment pauses loading at several predefined cycle intervals. During these pauses, a low-speed, small-amplitude quasi-static load is applied to the specimen, and the corresponding force-displacement relationship is recorded. The regression equation fitted to the experimental data reveals a linear relationship between force and displacement, with the slope of the equation, as shown in Figure 4, representing the stiffness value.

To ensure data accuracy, the specimen temperature is stabilized and loading conditions are kept consistent before resuming fatigue loading. This method not only captures high-frequency dynamic response information but also records the static stiffness degradation characteristics that evolve with the number of cycles. Consequently, the experimental data exhibit good temporal consistency and physical interpretability, providing a reliable foundation for constructing the rubber material damage evolution model and training the Physics-Informed Neural Network (PINN).

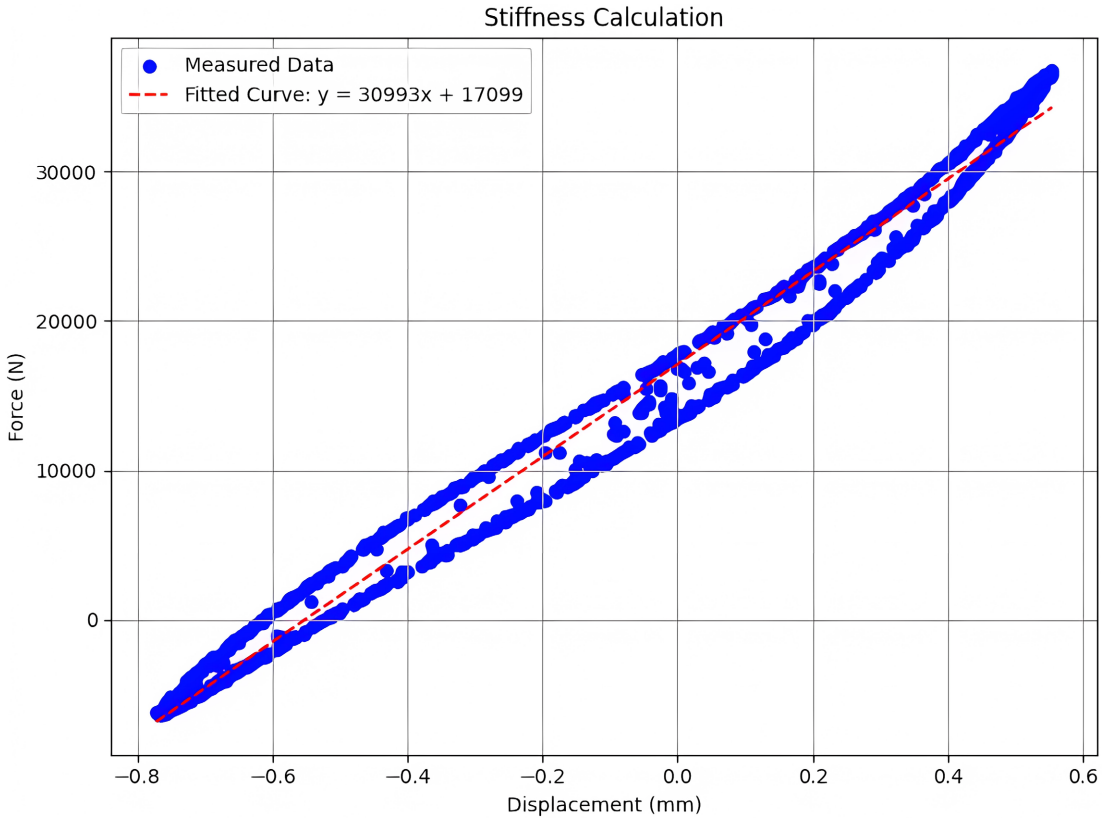

Figure 4. Stiffness measurement.

4. Results and Discussion

To validate the proposed PINN models in Section 2, the conventional BPNN was

implemented using the same data input for comparison. The division of training and test datasets is based on distinct physical specimens to evaluate the model's generalization capability. Specifically, data from specimens S1 to S5 are assigned to the training set, while specimens S6 and S7 are allocated to the test set. This setup enables assessment of the model's extrapolation performance in fatigue life prediction. All machine learning models were carried out in the TensorFlow framework and a workstation (CPU: Intel(R) Core(TM) i9-10900X CPU@3.70 GHz, RAM: 128.0 GB, and GPU: NVIDIA GeForce RTX 3060 Ti).

Analysis of the Predictive Performance

Figure 5 shows the comparison between the stiffness predicted by the BPNN model and the PINN model versus the actual stiffness on the test set. It can be observed that the BPNN model fails to accurately capture the stiffness change trend in the later stages of stiffness degradation, resulting in significant prediction errors. In contrast, the PINN model demonstrates higher accuracy throughout the entire prediction process. Particularly during the stiffness degradation period, the predictions from the PINN model closely align with the actual values, showing a stronger fitting capability. By incorporating the physical damage evolution equation, PINN effectively captures the nonlinear fatigue degradation process of rubber materials, providing more stable and reliable predictions.

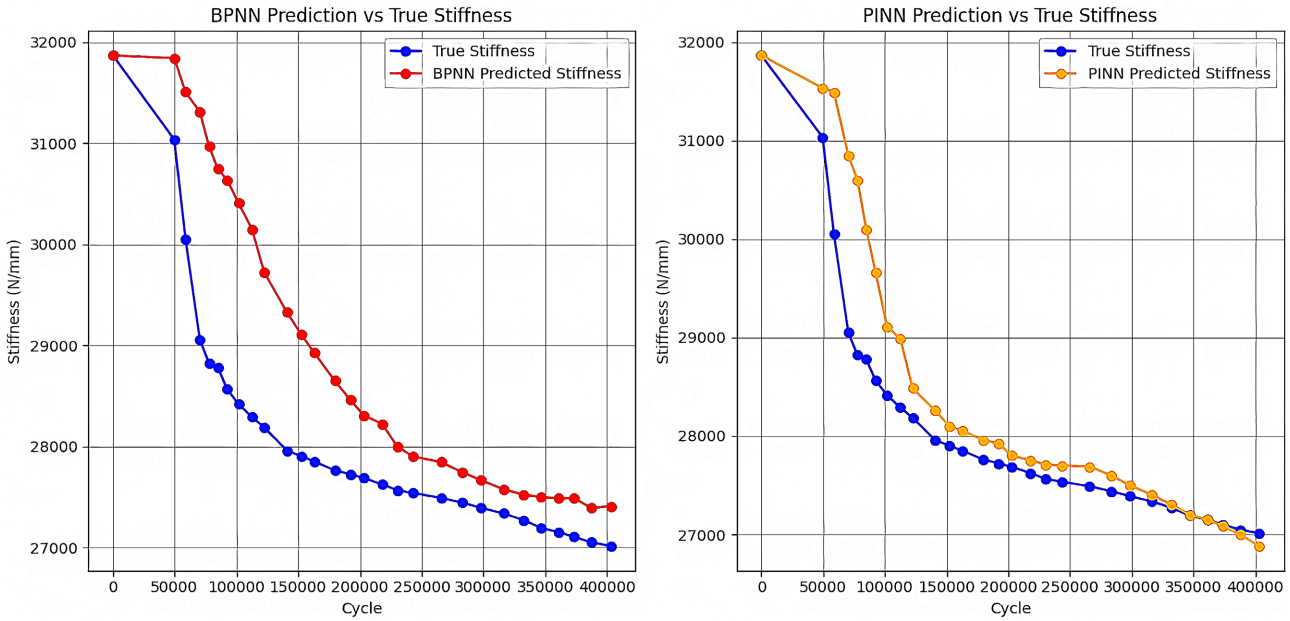

Figure 5. Comparison of stiffness predictions from BPNN and PINN on the validation set.

Figure 6 and Figure 7 display the relationship between the model's predicted values and the actual values, helping us assess the prediction ability and error magnitude of the models. By observing the fitting performance of both the BPNN and PINN models on the training and test datasets, we can evaluate their prediction accuracy. On the training set, the BPNN model shows relatively good fitting

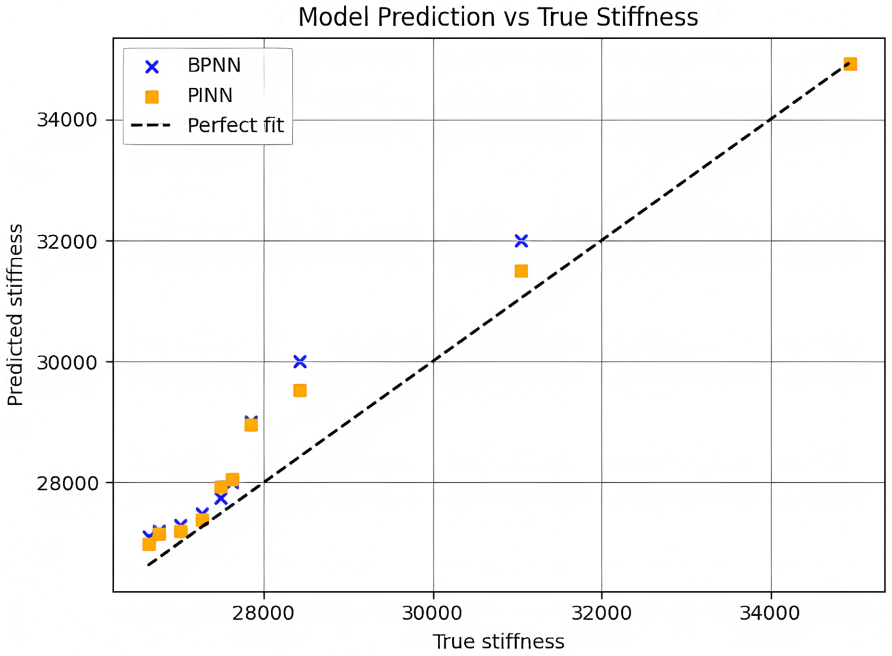

Figure 6. Comparison of stiffness prediction errors for BPNN and PINN on the training set.

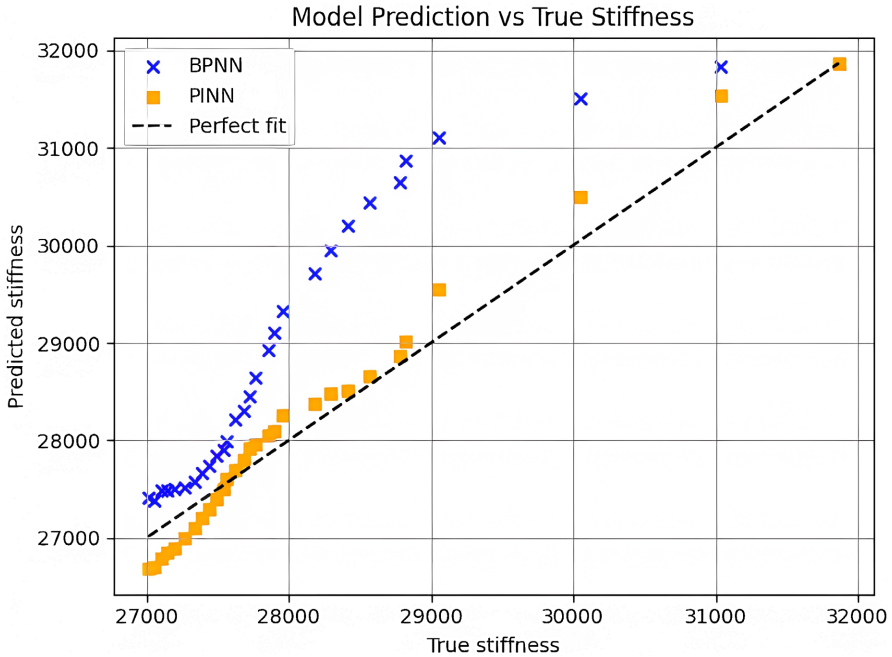

Figure 7. Comparison of stiffness prediction errors for BPNN and PINN on the test set.

performance. However, on the test set, as the data complexity increases, the prediction error gradually increases, especially in the region of rapid stiffness degradation. This indicates that the BPNN model performs poorly when dealing with high stiffness degradation or nonlinear changes. In contrast, the PINN model exhibits better prediction performance on both the training and test sets. Notably, on the test set, the PINN model effectively captures the stiffness variation trend,

maintaining high prediction accuracy even in regions of high stiffness and fatigue degradation. By comparing the two figures, it is evident that the PINN model's predictions consistently align more closely with the actual values, especially in the regions of high stiffness and fatigue degradation, showing more stable performance.

To further evaluate the performance of BPNN and PINN, RMSE and the coefficient of determination (R^2) are used as metrics for assessing prediction accuracy. Their calculation formulas are given as follows:

$$\mathrm{RMSE} = \sqrt{\frac{1}{n}\sum_{i=1}^{n}\left(y_{\mathrm{true}}^{(i)} - y_{\mathrm{pred}}^{(i)}\right)^2} \tag{16}$$

$$R^2 = 1 - \frac{\sum_{i=1}^{n}\left(y_{\mathrm{true}}^{(i)} - y_{\mathrm{pred}}^{(i)}\right)^2}{\sum_{i=1}^{n}\left(y_{\mathrm{true}}^{(i)} - \bar{y}_{\mathrm{true}}\right)^2} \tag{17}$$

where n is the number of samples; $y_{\mathrm{true}}^{(i)}$ is the true stiffness of the i-th sample; $y_{\mathrm{pred}}^{(i)}$ is the stiffness predicted by the model for the i-th sample; and $\bar{y}_{\mathrm{true}}$ is the mean of the true values.

Table 2. Estimation results of BPNN and PINN on different datasets (%).

Model Index	BPNN		PINN	
	RMSE	R^2	RMSE	R^2
Train	745.79	0.9307	602.16	0.9425
Test	1137.75	0.0073	646.35	0.9398

Root Mean Square Error (RMSE) is a commonly used evaluation metric for regression models, especially in prediction models, to measure the difference between the predicted and actual values. A smaller RMSE value indicates that the model has a smaller error and a better fit when predicting stiffness degradation during the fatigue process. The coefficient of determination (R^2) represents the proportion of the variance in the output variable that can be explained by the input variables. A value close to 1 indicates a better model fit and more accurate predictions. Table 2 provides the RMSE and R^2 values for the BPNN and PINN models for both training and testing samples. The results show that BPNN exhibits poor predictive performance on the test samples and fails to generalize effectively. In contrast, PINN, due to the incorporation of physical damage constraints, demonstrates lower RMSE and higher R^2 values on both the training and testing samples, indicating that physical information enhances the model's predictive performance and generalization ability.

5. Conclusions

This study investigates a fatigue life prediction method for elastic rubber support components. The main findings of this study are as follows:

1) The study conducted uniaxial fatigue tests on multiple rubber support components using an electro-hydraulic servo system. The displacement and stiffness data of the specimens under different cyclic loads were recorded in real-time, and the fatigue life of the rubber components was determined using stiffness degradation curves. Based on these experimental data, both a Physics-Informed Neural Network (PINN) model and a traditional pure data-driven model (BPNN) were developed for fatigue life prediction.

2) Model training results show that by incorporating physical constraints, the PINN model not only improves prediction accuracy but also demonstrates stability and robustness with small sample data, showing strong potential for practical applications. The PINN model exhibits lower MSE and RMSE, and higher R^2 values on both the training and testing sets compared to BPNN, indicating stronger generalization ability on the test set. In contrast, BPNN shows a significant increase in prediction error and a lower R^2 value on the test set, indicating poor generalization ability and clear overfitting issues.

This study provides an efficient and physically consistent modeling approach for the fatigue life assessment of rubber-based support components. The approach is widely applicable in engineering design and reliability evaluation, particularly when dealing with complex nonlinear degradation processes, offering advantages over traditional empirical models and data-driven models. The experimental basis of this study is relatively narrow. This may limit the generalization of conclusions to material variability and broader operating conditions. Although the advantages of PINN with small-sample data have been demonstrated, future work could incorporate more specimens. It could also include diverse loading and temperature conditions. This would further validate the model's robustness.

Conflicts of Interest

The authors declare no conflicts of interest regarding the publication of this paper.

References

[1] Yao, Q.Y., Dong, P., Zhao, Z.Y., *et al.* (2023) Temperature Dependent Tensile Fracture Strength Model of Rubber Materials Based on Mooney-Rivlin Model. *Engineering Fracture Mechanics*, **292**, Article 109646. https://doi.org/10.1016/j.engfracmech.2023.109646

[2] Liu, X.N., Zhao, X.Z. and Liu, X.A. (2023) A Unified Probabilistic Fatigue Life Prediction Model for Natural Rubber Components Considering Strain Ratio Effect. *Fatigue & Fracture of Engineering Materials & Structures*, **46**, 1473-1487. https://doi.org/10.1111/ffe.13941

[3] Cheng, Z.X., Wang, H. and Wang, P. (2022) A Multi-Grid Sampling Multi-Scale Method for Crack Initiation and Propagation. *Engineering Fracture Mechanics*, **271**, Article 108671. https://doi.org/10.1016/j.engfracmech.2022.108671

[4] Chong, Z.H., Yue, T.L., Yao, Q.L., *et al.* (2021) Experimental and Numerical Investigation of Crack Propagation in Bolting Systems Strengthened with Resin-Encapsulated Rock Bolts. *Engineering Failure Analysis*, **122**, Article 105259.

https://doi.org/10.1016/j.engfailanal.2021.105259

[5] Wang, X., Sedaghati, R., Rakheja, S. and Shangguan, W. (2025) Rubber Fatigue Revisited: A State-of-the-Art Review Expanding on Prior Works by Tee, Mars and Fatemi. *Polymers*, **17**, Article 918. https://doi.org/10.3390/polym17070918

[6] Zainalfirdaus, A., Chang, V.C., Ho, J.H., *et al.* (2025) Comparative Studies of Deep Learning Neural Network Architectures in Fault Diagnosis of Rubber Vibration Isolators. *Civil Engineering Infrastructures Journal*.

[7] Sun, Y.H., Liu, X.N., Yang, Q., *et al.* (2024) Improving Fatigue Life Prediction of Natural Rubber Using a Physics-Informed Neural Network Model. *Fatigue & Fracture of Engineering Materials & Structures*, **48**, 1039-1049. https://doi.org/10.1111/ffe.14533

[8] Liu, X.N. and Wang, X.L. (2023) Natural Rubber Components Fatigue Life Estimation through an Extreme Learning Machine. *Proceedings of the Institution of Mechanical Engineers, Part L: Journal of Materials: Design and Applications*, **237**, 81-91. https://doi.org/10.1177/14644207221102567

[9] Liu, X.N., Zhao, X.Z. and Shangguan, W.B. (2022) Fatigue Life Prediction of Natural Rubber Components Using an Artificial Neural Network. *Fatigue & Fracture of Engineering Materials & Structures*, **45**, 1678-1689. https://doi.org/10.1111/ffe.13690

[10] Liu, X.N., Zhao, X.Z. and Shangguan, W.B. (2022) Residual Fatigue Life Prediction of Natural Rubber Components under Variable Amplitude Loads. *International Journal of Fatigue*, **165**, Article 107199. https://doi.org/10.1016/j.ijfatigue.2022.107199

[11] Hottin, A., Naït Abdelaziz, M., Talha, A. and Charrier, P. (2023) Continuum Damage Mechanics to Predict Rubber Fatigue Life under Multiaxial Loadings. *International Journal of Fatigue*, **170**, Article 107559. https://doi.org/10.1016/j.ijfatigue.2023.107559

[12] Pan, Z., Lai, Y., Wang, Y., Duan, W., Qiao, Y., Liu, Y., *et al.* (2021) Fatigue Life Prediction and Effects of Cerium Oxide-Filled Vulcanized Natural Rubber on Fatigue Life under Multiaxial Loading. *Fatigue & Fracture of Engineering Materials & Structures*, **44**, 3349-3362. https://doi.org/10.1111/ffe.13561

[13] Tavosi, S., Alimardani, M., Ghoreishy, M.H.R. and Tavakol, M. (2024) Fatigue Failure Modeling in Rubber Stator of Downhole Motors: Dependency to Materials and Geometry, and Its Application to Life Prediction. *Engineering Failure Analysis*, **159**, Article 108072. https://doi.org/10.1016/j.engfailanal.2024.108072

[14] Robin, E., Le Cam, J.B., Delahaye, G., Ruellan, B., Di Cesare, N. and Canévet, F. (2025) A First Proposal for Fatigue Life Prediction of Carbon Black Filled Natural Rubber at Different Temperatures with an Artificial Neural Network. *Strain*, **61**, e70001. https://doi.org/10.1111/str.70001

[15] Bang, J., Choi, M., Lee, H., Jeong, S., Yoon, J. and Doh, J. (2025) Data-Efficient and Uncertainty-Aware RUL Prediction Using Physics-Informed Neural Networks. *Annual Conference of the PHM Society*, **17**, 1-12. https://doi.org/10.36001/phmconf.2025.v17i1.4356

[16] Liu, H., Ding, X., Liu, J., Zhang, Y., Zhang, B., Li, E., *et al.* (2025) A Physics-Informed Neural Network Model for Combined High and Low Cycle Fatigue Life Prediction. *Mechanics of Materials*, **209**, 105429. https://doi.org/10.1016/j.mechmat.2025.105429

[17] Chen, J. and Liu, Y. (2022) Fatigue Modeling Using Neural Networks: A Comprehensive Review. *Fatigue & Fracture of Engineering Materials & Structures*, **45**, 945-979.

[18] Wang, L., Zhu, S., Luo, C., Niu, X. and He, J. (2023) Defect Driven Physics-Informed

Neural Network Framework for Fatigue Life Prediction of Additively Manufactured Materials. *Philosophical Transactions of the Royal Society A*: *Mathematical*, *Physical and Engineering Sciences*, **381**, Article 20220386. https://doi.org/10.1098/rsta.2022.0386

[19] Halamka, J., Bartošák, M. and Španiel, M. (2023) Using Hybrid Physics-Informed Neural Networks to Predict Lifetime under Multiaxial Fatigue Loading. *Engineering Fracture Mechanics*, **289**, Article 109351. https://doi.org/10.1016/j.engfracmech.2023.109351

[20] Wang, H., Li, B., Gong, J. and Xuan, F. (2023) Machine Learning-Based Fatigue Life Prediction of Metal Materials: Perspectives of Physics-Informed and Data-Driven Hybrid Methods. *Engineering Fracture Mechanics*, **284**, Article 109242. https://doi.org/10.1016/j.engfracmech.2023.109242

[21] Chen, D., Li, Y.Z., Liu, K. and Li, Y. (2023) A Physics-Informed Neural Network Approach to Fatigue Life Prediction Using Small Quantity of Samples. *International Journal of Fatigue*, **166**, Article 107270. https://doi.org/10.1016/j.ijfatigue.2022.107270

[22] Dong, Y.X., Yang, X.F., Chang, D.D. and Li, Q. (2025) Predicting Fatigue Life of Multi-Defect Materials Using the Fracture Mechanics-Based Physics-Informed Neural Network Framework. *International Journal of Fatigue*, **190**, Article 108626. https://doi.org/10.1016/j.ijfatigue.2024.108626

[23] Li, Z., Dai, W., Yue, H., Guo, C., Ji, Z., Li, Q., *et al.* (2025) Fatigue Life Prediction of 2024-T3 Clad Al Alloy Based on an Improved SWT Equation and Machine Learning. *Materials*, **18**, Article 332. https://doi.org/10.3390/ma18020332

[24] Luo, R.K. (2024) Fatigue Prediction Criteria for Rubber Antivibration Design with Temperature Effects. *International Journal of Fatigue*, **183**, Article 108271. https://doi.org/10.1016/j.ijfatigue.2024.108271

[25] Wang, C., Huang, Z., He, C., Lin, X., Li, C. and Huang, J. (2025) Research on Remaining Useful Life Prediction Method for Lithium-Ion Battery Based on Improved GA-ACO-BPNN Optimization Algorithm. *Sustainable Energy Technologies and Assessments*, **73**, Article 104142. https://doi.org/10.1016/j.seta.2024.104142

[26] Ma, T., Jing, G.X., Sun, X.X., Chen, G., *et al.* (2025) Low-Cycle and Thermomechanical Fatigue Life Prediction Method for Compacted Graphite Iron Based on Small-Sample Physics-Informed Neural Networks. *Fatigue & Fracture of Engineering Materials & Structures*, **48**, 3999-4016. https://doi.org/10.1111/ffe.70002

[27] Zhang, Q., Liu, Z., Yang, G., Jing, Y., Shu, Y. and Zha, S. (2025) Deep Learning-Based Calibration Method for Material Parameters of Resilient Wheel Rubber Components. *Polymer*, **319**, Article 128044. https://doi.org/10.1016/j.polymer.2025.128044

[28] Zhang, Z., Zhou, Y. and Vassiliou, M.F. (2023) Experimental, Numerical, and Theoretical Studies on Vertical Stiffness Reduction of Lead Thick Rubber Bearings. *Construction and Building Materials*, **384**, Article 131421. https://doi.org/10.1016/j.conbuildmat.2023.131421

[29] Zhou, Y., Zhang, Z. and Vassiliou, M.F. (2022) Investigation on Vertical Stiffness Reduction of Thick Rubber Bearings under Lateral Displacement. *Construction and Building Materials*, **360**, Article 129563. https://doi.org/10.1016/j.conbuildmat.2022.129563